


## Aeroelastic Analysis of a Smart Sandwich Compressor Blade with Electrorheological Core

Shahrokh Shams <sup>\*</sup>, Sajad Jangravi, Mohammad Reza Kazemi

School of Aerospace Engineering, College of Interdisciplinary Science and Technology, University of Tehran, Tehran, Iran.

### ARTICLE INFO

#### Article Type

Original Research

#### Article History

Received: January 07, 2025

Revised: October 05, 2025

Accepted: November 16, 2025

ePublished: November 30, 2025

### ABSTRACT

Torsional aero-elastic analysis as well as the effect of the bending-torsion coupling on flutter stability boundaries of a turbomachinery cascade with electrorheological (ER) smart fluid based sandwich blade are studied. The governing equation of bending and torsional motion is based on classical sandwich beam theory and also the torsional theory of laminated rectangular plate have been used to formulate the structural dynamics of the blade in torsional mode. The electrorheological smart fluid is used as a middle layer between two elastic layers to investigate the effect of this electrorheological fluid on the aero-elastic behavior of the blades. Unsteady Whitehead's aerodynamic theory applied to model aerodynamic loadings. Lagrange equation and the assumed mode method are employed for discretization and derive the governing equation of the system. The results show the acceptable effect of adding smart fluid as a middle layer on the aero-elastic behavior and stability of mistuning blades. In fact, the aim of this study is to investigate the effect of electrorheological (ER) smart fluid on aeroelastic behavior of a sandwich beam with electrorheological core and elastic constraining layers. Observations showed that adding this fluid to the system can also be considered as a passive method in controlling vibrations and delaying the flutter phenomenon. by increasing the electric field intensity from 2 to 4, the dimensionless flutter speed increases by 22.2%.

**Keywords:** Torsional Vibration, Rotary Smart Sandwich Blade, Electrorheological Core

### How to cite this article

Shams Sh, Jangravi S, Kazemi M.R, Aeroelastic Analysis of a Smart Sandwich Compressor Blade with Electrorheological Core. Modares Mechanical Engineering; 2025;25(11):747-758.

*\*Corresponding author's email: shahrokh.shams@ut.ac.ir*

*\*Corresponding ORCID ID: 0000-0002-1259-821X*



Copyright© 2025, TMU Press. This open-access article is published under the terms of the Creative Commons Attribution-NonCommercial 4.0 International License which permits Share (copy and redistribute the material in any medium or format) and Adapt (remix, transform, and build upon the material) under the Attribution-NonCommercial terms.

## 1- Introduction

Aeroelasticity is a notably new branch of applied mechanics that studies the interaction between fluid matters and flexible solid bodies. In the context of aircraft structures, this field is defined as the study of phenomena that arise from the interaction of aerodynamic, inertial, and elastic forces during the relative motion of a fluid (air) and a flexible body (aircraft) [1–4].

Forced responses due to aerodynamic loading and the flutter phenomenon are among the most important concerns in turbomachine applications. Neglecting these issues may lead to significant financial losses. Aero-elastic flutter, defined as “an unstable, self-excited structural oscillation at a definite frequency where energy is extracted from the airstream by the motion of the structure,” is ubiquitous in many engineering fields. When flutter occurs, the blade vibrates with high amplitude and may eventually fail.

Smart materials, such as Electrorheological (ER) and Magnetorheological (MR) fluids, have gained considerable attention in recent research. Electrorheological fluid is a suspension of non-conducting particles in an insulating liquid, highly sensitive to electric fields. When exposed to an external electric field, the suspended particles react quickly, altering the rheological properties of the fluid. Upon removal of the field, the fluid can return to its original state. Due to its shear modulus, ER fluid can be considered viscoelastic and is suitable for vibration control in structures.

By placing ER fluid between two elastic layers, a sandwich structure can be created to control vibrations and delay the onset of flutter. Historical studies support this idea. In the late 1950s and early 1960s, Kerwin [5] introduced a damping model using a viscoelastic layer, demonstrating positive effects on energy dissipation and good alignment with experimental data.

In 1999, Qiu et al. [6] studied the effect of ER fluid on the damping factor of multilayer beams. Their findings showed a significant increase in damping with increased electric field strength, along with an increase in the natural frequency due to stiffness changes in the ER fluid layers. Similarly, Kang et al. [7] investigated both active and passive characteristics of composite beams containing ER fluid. Their results revealed that applying an electric field leads to more efficient active damping in flexible laminated beams compared to stiff ones.

Wei et al. [8] analyzed the dynamics of rotating ER composite beams using a three-layer model (an ER middle layer and two elastic outer layers) and finite element methods. They reported increased damping and reduced vibration amplitudes under electric fields. Ariloglu and Ozkol [9] explored vibrations in composite sandwich beams with a viscoelastic core using the differential transform method and Hamilton's principle. Their solutions matched well with previous studies.

Allahverdizadeh et al. [10] examined the vibration behavior of functionally graded ER sandwich beams, utilizing both experimental and analytical approaches. Their optimized FE model was used to assess the effects of electric field, volume fraction index, and boundary conditions on the dynamic response of adaptive sandwich beams.

In the field of turbomachinery aero-elasticity, Marshall and Imergan (1996) [11] presented a comprehensive study on aero-elastic instability methods in turbomachine blades. Whitehead [12] examined unstalled bending flutter in turbomachinery blade cascades, concluding that deviations in steady flow can cause phase differences in blade motion, resulting in flutter.

Rahiminasab [13] investigated the aero-elastic stability of smart sandwich plates with ER fluid cores and orthotropic faces. Brahimi and Ouibrahim [14] analyzed the dynamic blade response due to fluid–structure interaction in turbomachinery. Their simulations indicated that pressure rate influences aero-elastic instabilities. Bornassi et al. [15] studied coupled bending–torsion flutter in MRE tapered sandwich blades using Whitehead's theory. Their findings

confirmed that both the interaction between bending and torsion and changes in cross-sectional area significantly affect flutter stability.

Another widely used method to improve aero-elastic behavior in turbomachinery is mistuning. This technique involves deliberate small deviations in blade parameters (e.g., natural frequency) to delay flutter instability. Kaza and Kielb [16] employed Whitehead's aerodynamic theory to study mistuning effects on aero-elastic instability and forced responses in blade cascades under compressible flow. Their results showed mistuning enhances flutter resistance in both coupled and uncoupled modes. They extended their work [17] to subsonic and ultrasonic regimes, comparing effects of random and alternating mistuning patterns on flutter behavior.

Like the use of ER fluids, mistuning is considered a passive control technique. However, based on the author's knowledge, no prior research has addressed aero-elastic behavior of turbomachine blades using electrorheological smart fluid.

Recent studies outside the turbomachinery field show promising potential for ER fluids in rotating machinery. Mutra and Srinivas [18] examined semi-active vibration control of high-speed turbocharger rotors using ER fluid as lubricant in floating ring bearings. Their findings showed that electric fields dynamically adjust viscosity, reducing rotor vibrations and enhancing system stability at high speeds.

Sakly and Chouchane [19] investigated electro-rheological elastomer (ERE) rings in rotor–bearing systems, demonstrating their effectiveness in reducing vibrations under both steady and transient conditions. They concluded that electric fields improve stiffness and modify resonance frequencies, making ERE rings valuable for vibration suppression.

Lastly, Sun and Thomas [20] developed a smart ER dynamic absorber to regulate torsional vibrations in rotor systems. By using ER fluid to dynamically adjust damping and stiffness, they introduced a promising solution for vibration control.

In this paper we use smart electrorheological fluid as the intermediate bound layer and using the theory of torsion for rectangular laminated plates for torsional vibrations, Hamilton's principle for bending vibrations and also using Whitehead's un-steady aerodynamic theory to model the aerodynamics and finally solve the governing equation by Using the assumed modes method, the aero-elasticity of a row of turbomachinery blades is studied. In this study, we seek to study the effect of electrorheological (ER) smart fluid on aeroelastic behavior of a sandwich beam with electrorheological core and elastic constraining layers.

## 2- Modeling and governing equations

First it is assumed that there is no slip between the layers and the middle layer is well placed in the between. Because the young modulus of the smart middle layer is negligible compared to the elastic layers, normal stress and strain are neglected. However, the strain energy stored in the smart layer is significant. Also, due to the considerable density of the smart middle layer, the effect of this fluid on the kinetic energy in the longitudinal direction must be considered. Based on the studies on the elastic behavior of ER fluid [21, 22], two distinct behaviors can be considered for this fluid as the post-yield and pre-yield regimes. Figure 1, shows the typical stress-strain curve of a smart fluid like ER fluid in a particular response to an electric or magnetic field.

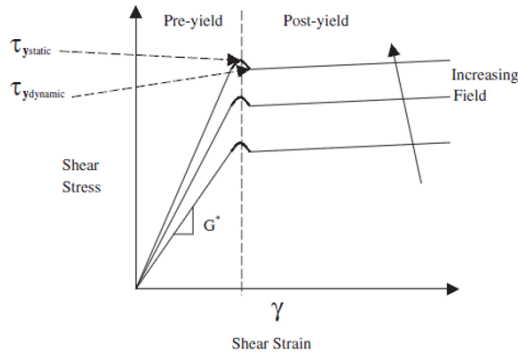


**Fig.1** Shear stress-shear strain behavior of smart materials under different intensities of the electric field [23]

Electrorheological fluids in the pre-yield regime behave similarly to viscoelastic materials, exhibiting both elastic and viscous behavior. As a result, the behavior of the intelligent fluid in the pre-Yield regime in according to the linear viscoelastic theory is as follows [23]:

$$\tau(t) = G^* \gamma \quad (1)$$

Shear stress is related to shear strain by a complex shear modulus, which is defined as follows:

$$G^* = G' + iG'' \quad (2)$$

In equation (2),  $G'$  is the storage modulus and  $G''$  is the loss modulus. The storage modulus indicates the average potential energy per unit volume and the loss modulus shows the damping of energy dissipated in each cycle. With the following definition:

$$\eta_c = \frac{G''}{G'} \quad (3)$$

The equation (3) can be reconsidered as:

$$G^* = G'(1 + i\eta_c) \quad (4)$$

Where  $\eta_c$  is the material damping factor and is stated as the ratio of the loss modulus to the storage modulus.

The characteristics of the electrorheological smart fluid studied in this study are extracted according to the following equation and based on the applied voltage [24].

$$G'(E) = m_g E + b_g \quad (5-a)$$

$$\eta_c(E) = m_e E + b_e \quad (5-b)$$

Where  $m_g = 1500 \text{ pa}$ ,  $b_g = 0$  and  $b_e = 3.73 \text{ pa.s}$ ,  $m_e = 270 \text{ mpa.s} \cdot \frac{\text{mm}}{\text{kV}}$ .

## 2-1- Tuned and Mistuned Cascades

In a tuned cascade, the vibration amplitude of all the blades is the same and their mechanical properties are similar. There are  $N$  modes for the cascade, which is called the interblade phase angle. The number of interblade phase angles is calculated based on the Lane assumption [25]:

$$\beta_r = \frac{2\pi r}{N}, r=0, \dots, N-1 \quad (6)$$

The blades of a mistuned cascade have different properties and their amplitude of vibrations is not the same [25]. In this cascade, the blade response can be assumed in the form of a combination of linear series of possible motions in the interblade phase angle modes in the tuned cascade.

$$q_s e^{i\omega t} = \sum_{r=0}^{N-1} q_{ar} e^{i(\omega t + \beta_r s)} \quad s=1, 2, \dots, N-1 \quad (7)$$

$q_s$  Represents the amplitude of vibrations of the  $s$ th blade and  $q_{ar}$  denotess the amplitude of vibrations in the  $r$ th interblade phase angle mode. equation (5) can be rewritten in matrix form:

$$q e^{i\omega t} = E q_a e^{i\omega t} \quad (8)$$

In which

$$q = \begin{bmatrix} q_0 \\ q_1 \\ \vdots \\ q_{N-1} \end{bmatrix}, q_a = \begin{bmatrix} q_{a0} \\ q_{a1} \\ \vdots \\ q_{aN-1} \end{bmatrix}, E = \begin{bmatrix} E(0,0)I & \dots & E(0,N-1)I \\ \vdots & \ddots & \vdots \\ E(N-1,0)I & \dots & E(N-1,N-1)I \end{bmatrix} \quad (9)$$

That  $(s,r) = e^{2\pi i s r / N}$ .

The  $I$  matrix's dimensions is dependent of the number of the generalized coordinates used to describe the blade's motion, and is a square identity.

## 2-2- Structural model

Figure 2 presents a schematic representation of the problem, featuring a row of blades mounted on a disk. Each blade comprises a three-layer sandwich structure made of electrorheological core and elastic constraining layers.

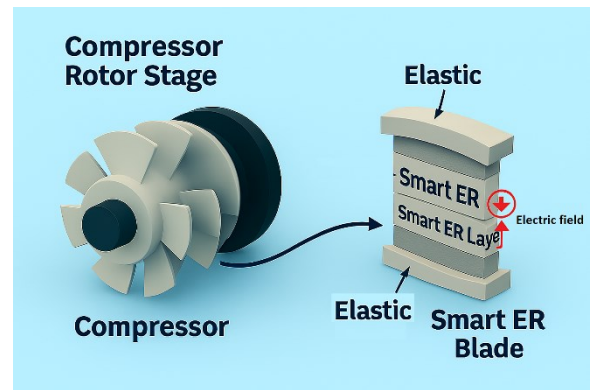


**Fig.2** The general schematic of the problem

The blade with length  $L$ , width  $2b$ , thickness  $h$ , fixed setting angle  $\zeta$ , disk radius  $R$  and rotational speed is  $\Omega$  is shown in Figure 3. The assumed three-layer beam, including two elastic layers at the top and bottom, and a smart ER layer is also located between these two elastic layers.

To investigate the behavior of the sandwich blade and according to Figure 3, it will be assumed that shear strains in the face plates are negligible and that longitudinal direct stresses in the core are negligible. The thickness of all layers is very small comparing to the length of the blade and there is no slippage and delamination between the elastic layers and the electrorheological elastomer layer.

Additional basic assumptions are listed as follows:

- Compared to elastic layers, the Young's modulus of the middle layer is negligible and the stress and strain of this layer in the vertical direction are ignored.
- Since the cross-sectional area is symmetrical, then only aerodynamic loads cause the torsional and bending motion coupling and are structurally uncoupled.
- All three layers have the same displacement in the transverse direction( $z$ ).

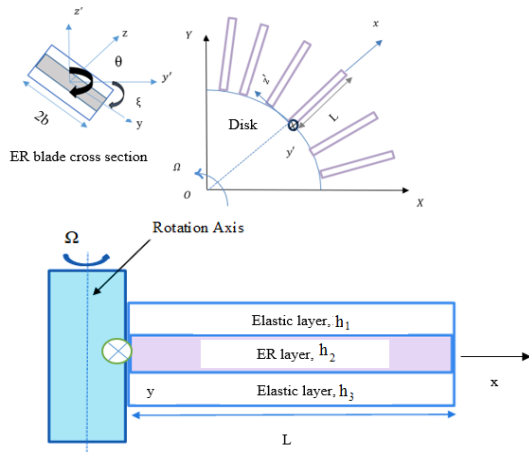


Fig.3 Configuration of blade with ER core

### 2-2-1- Torsional vibration

Torsional vibration is defined using the torsional theory of laminated sandwich beams [26]. The potential energy generated by the shear and axial deformation due to torsional vibrations in the sandwich beam can be written as follows [26]:

$$U_1 = \frac{1}{2} \int_0^L I_1 \theta'^2 dx + \frac{1}{2} \int_0^L I_2 \theta''^2 dx \quad (10)$$

In equation (10), theta represents the torsional motion of the cross-section of the beam around the X-axis. In addition, the torsional constant  $I_1$  and longitudinal rigidity  $I_2$  of the sandwich beam are defined as follows:

$$I_1 = \frac{1}{\theta} \iint_A (y\sigma_{xz} - z\sigma_{xy}) dA \quad (11-a)$$

$$I_2 = \iint_A E_k \Psi_k^2 dA \quad (11-b)$$

Which  $\Psi_k$  represents the warping function and  $\sigma_{xz}$  and  $\sigma_{xy}$  are also elements of shear stress and  $E_k(1,2,3)$  indicates young's modulus of top and bottom elastic layers. The warping function is written as follows [26]:

$$\begin{aligned} \Psi_k(x,y,z) &= yz - \frac{(2b)^2}{\sqrt{G_{xyk} G_{xzk}}} \sum_{m=0}^{\infty} \frac{8(-1)^m}{\pi^3(2m+1)} \\ &+ [A_{km} \sinh(\beta_{km} \frac{z}{h}) + B_{km} \cosh(\beta_{km} \frac{z}{h})] \sin \left( (2m+1) \frac{\pi y}{2b} \right) \end{aligned} \quad (12)$$

That  $\beta_{km} = (2m+1) \frac{\pi h}{2b} \sqrt{\frac{G_{xyk}}{G_{xzk}}}$  and  $h = h_1 + h_2 + h_3$ .

The kinetic energy resulting from torsional vibrations is obtained as follows [27]:

$$T_1 = \int_0^L I_3 \dot{\theta}^2 dx + \int_0^L I_4 \dot{\theta}^2 dx \quad (13)$$

Where:

$$\begin{aligned} I_3 &= I_a + I_b \\ I_a &= \iint \rho_k y^2 dA \\ I_b &= \iint \rho_k z^2 dA \end{aligned} \quad (14)$$

And,

$$I_k = \iint \rho_k \Psi_k^2 dA \quad (15)$$

$\rho_k$ , is the corresponding density to any layer.

### 2-2-2- Bending- axial vibration

According to Figure 4, the bending vibrations of the elastic layers in the z direction follow Bernoulli's Euler beam theory [8]. Based on this theory, the potential energy due to the bending displacement (w) and axial displacements ( $u_1, u_3$ ) of the elastic layers is written as follows [24]:

$$\begin{aligned} U_2 &= \frac{1}{2} \int_0^L (A_1 E_1 u_{1,x}^2 + A_3 E_3 u_{3,x}^2) dx + \\ &+ \frac{1}{2} \int_0^L (E_1 I_1 + E_3 I_3) w^2 dx + \frac{1}{2} \int_0^L G^* A_2 \gamma^2 dx \end{aligned} \quad (16)$$

The last phrase in this equation indicates the potential energy that is related to the shear deformation due to the linear viscoelastic behavior,  $A_k (k=1,2,3)$  designates the cross-sectional area,  $I_k (k=1,2,3)$  is the second moment of area.

The shear strain of the smart middle layer resulting from bending and axial displacements is as describes [28]:

$$\gamma = \frac{u_1 - u_3}{h_2} + w_{,x} + \frac{h_1 + h_3}{2h_2} w_{,x} \quad (17)$$

$u_k (k=1,2,3)$  denotes the longitudinal displacements of layers.

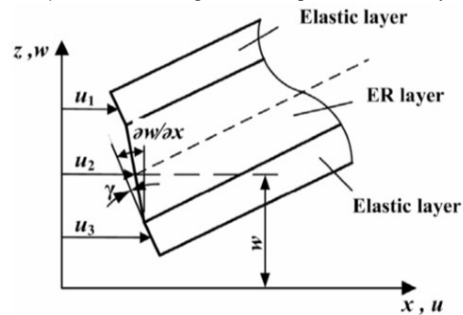


Fig.4 Longitudinal-bending displacements of three-layer beams [24]

The kinetic energy due to longitudinal and bending displacements in the beam is obtained as follows:

$$\begin{aligned} T_2 &= \int_0^L \rho w^2 A dx + \frac{1}{2} \int_0^L (\rho_1 A_1 \dot{u}_1^2 + \rho_3 A_3 \dot{u}_3^2) dx \\ &+ \frac{1}{2} \int_0^L \rho^2 I_{2y} \dot{\gamma}^2 dx \end{aligned} \quad (18)$$

Where  $\rho A = \rho_1 A_1 + \rho_2 A_2 + \rho_3 A_3$ .

The last expression of this equation represents the kinetic energy due to the rotation of the smart ER middle layer.

To elaborate further, the influence of the electric field on the governing equations of motion is explicitly incorporated in Equation (12) for torsional vibrations and Equation (16) for bending vibrations. In equation (12) the  $G^* = G_{xy2}$  and in equation (16) the  $G^*$  has been used in  $\frac{1}{2} \int_0^L G^* A_2 \gamma^2 dx$  relation. The electrorheological smart fluid properties, which are central to these formulations, are clearly defined in Equation (5).

### 2-2-3- Rotating speed effect

If the blades are connected to the cascade at a setting angle, the kinetic energy of the rotating beam is as follow [24, 27]:

$$T_3 = \frac{1}{2} \int_0^L \rho A \Omega^2 \cos^2(\xi) w^2 dx + \frac{1}{2} \Omega^2 \int_0^L (\cos^2(\xi) I_a + \sin^2(\xi) I_b) \theta^2 dx + \frac{1}{2} \Omega^2 \int_0^L I_4 \theta'^2 dx \quad (19)$$

The work done by the centrifugal forces is written as follows:

$$W_c = -\frac{1}{2} \int_0^L P(x) w'^2 dx - \frac{1}{2} \int_0^L P(x) I_5 \theta''^2 dx - \frac{1}{2} \int_0^L P(x) I_6 \theta'^2 dx \quad (20)$$

Where

$$I_5 = \iint \psi_k^2 dA \quad (21)$$

$$I_6 = \iint (y^2 + z^2) dA$$

$P(x)$  represents the centrifugal force per unit area and in section  $x$  is defined as [24].

$$P(x) = \rho A \Omega^2 (Rl + \frac{l^2}{2} - Rx - \frac{x^2}{2}) \quad (22)$$

### 2-3- Aerodynamic model

Aerodynamic forces are obtained using Whitehead's unsteady aerodynamic theory [29]. The blades are considered two-dimensional. The bending and torsional motion of the blade is considered in the form of two degrees of freedom of bending and torsion and only the bending motion perpendicular to the chord is considered and the bending vibrations in the chord direction are excluded.

The blades are considered as flat plates without thickness and the curvature of the airfoil is omitted. Also The blades are not in a stall condition. In fact, the fluid is not in the separation state and always remains attached to the surface.

The aerodynamic moment and lift are written in the form of a traveling wave as follows [17]:

$$L_s = -\pi \rho b^3 \omega^2 \sum_{r=0}^{N-1} \left[ l_{hr} \frac{h_{ar}}{b} + l_{\theta r} \theta_{ar} \right] e^{i(\omega t + \beta_r s)} \quad (23-a)$$

$$M_s = \pi \rho b^4 \omega^2 \sum_{r=0}^{N-1} \left[ l_{\theta r} \frac{h_{ar}}{b} + l_{\theta \theta r} \theta_{ar} \right] e^{i(\omega t + \beta_r s)} \quad (23-b)$$

Where  $h_{ar}$  and  $\theta_{ar}$  express the blade bending and torsional amplitudes in the  $r$ th inter-blade phase angle, in addition  $l_{hr}$ ,  $l_{\theta r}$ ,  $l_{\theta \theta r}$ , and  $l_{\theta \theta r}$  are nondimensional aerodynamic coefficients, and are stated as [29]:

$$l_{hr} = \frac{2i}{k} C_{Fq} \quad (24)$$

$$l_{\theta r} = \frac{2}{k^2} C_{F\theta} - i\lambda b C_{Fq}$$

$$l_{\theta \theta r} = \frac{4i}{k} C_{Mq} - b C_{Fq}$$

$$l_{\theta \theta r} = \frac{4}{k^2} C_{M\theta} - b C_{Fq} - i\lambda b C_{Mq} + i\lambda b^2 C_{Fq}$$

Where  $\lambda = 2k$ ,  $b = \frac{1+a}{2}$ ,  $k = \frac{b\omega}{U}$ .

Coefficients  $C_{Fq}$ ,  $C_{F\theta}$ ,  $C_{Mq}$  and  $C_{M\theta}$  are calculated by reduced frequency  $k$ , the inter-blade phase angle  $\beta_r$ , the ratio of the distance to the cord length of each blade, and the stagger angle  $\xi$ . Also,  $U$  is the flow velocity related to the blade,  $b$  is cord's blade and  $a$  is the distance between the elastic axis and the semi-cord. Considering the aerodynamic strip theory, the work because of non-conservative aerodynamic loadings is acquired by integrating the lift and moment over the blade span.

$$W_a = \int_0^L (-\bar{L}w(x,t) + \bar{M}\theta(x,t)) dx \quad (25)$$

### 2-4- Governing equations and analysis method

To derive the equations of motion of the bending-torsion coupling system, the Lagrange equations and assumed mode method are used. The system response is appraised in a linear combination form of permissible functions.

$$u_1(x,t) = \sum_{i=1}^n \Phi_{bi}(x) q_{1i}(t)$$

$$u_3(x,t) = \sum_{i=1}^n \Phi_{bi}(x) q_{2i}(t)$$

$$w(x,t) = \sum_{i=1}^n \Phi_{bi}(x) q_{3i}(t)$$

$$\theta(x,t) = \sum_{i=1}^n \Phi_{\theta i}(x) q_{5i}(t) \quad (26)$$

Where  $\Phi_{bi}$  and  $\Phi_{\theta i}$  are respectively the bending and torsional vibration mode shape that satisfy the geometric boundary conditions, and  $q_{1i}(t)$ ,  $q_{2i}(t)$ ,  $q_{3i}(t)$  and  $q_{5i}(t)$  are the generalized coordinates of the system. Also,  $n$  is the number trial function.

The Lagrange functions are defined as follows:

$$\frac{d}{dt} \left( \frac{\partial T_b}{\partial \dot{q}_i} \right) - \frac{\partial T_b}{\partial q_i} + \frac{\partial (U_b - W_b)}{\partial q_i} = 0 \quad (27)$$

Using Lagrange equations, the governing equation of motion of the system is derived as follows:

$$\mathbf{M}\ddot{\mathbf{q}} + \mathbf{K}\mathbf{q} = \omega^2 \mathbf{E} \mathbf{A} \mathbf{q}_a e^{i\omega t} \quad (28)$$

$\mathbf{A}$ ,  $\mathbf{K}$  and  $\mathbf{M}$  are respectively the aerodynamic, stiffness and mass matrices, and are also diagonal  $\mathbf{q}$  is generalized coordinate vectors.

For better explanation, The expressions for the mass, stiffness and aerodynamic matrices of the above equation are given in the **Appendix** for the case where have only two blades and the number of two mode shapes.

supposing harmonic motion  $\mathbf{q} = \bar{\mathbf{q}} e^{i\omega t}$ , this equation can be written as Eigen value problem form as follow:

$$\mathbf{K}\bar{\mathbf{q}} = \mathbf{g} \mathbf{H} \bar{\mathbf{q}} \quad (29)$$

Where

$$\mathbf{H} = \mathbf{M} + \mathbf{E} \bar{\mathbf{A}} \mathbf{E}^{-1} \quad (30)$$

And the aerodynamic matrix ( $\bar{\mathbf{A}}$ ) is written as:

$$\bar{\mathbf{A}} = \begin{bmatrix} \pi \rho b^4 \mathbf{E} \mathbf{A}_{\theta\theta} \mathbf{E}^{-1} & \pi \rho b^3 \mathbf{E} \mathbf{A}_{\theta w} \mathbf{E}^{-1} & [0]_{\theta u_1} & [0]_{\theta u_3} \\ \pi \rho b^3 \mathbf{E} \mathbf{A}_{w\theta} \mathbf{E}^{-1} & \pi \rho b^2 \mathbf{E} \mathbf{A}_{ww} \mathbf{E}^{-1} & [0]_{wu_1} & [0]_{wu_3} \\ [0]_{u_1\theta} & [0]_{u_1w} & [0]_{u_1u_1} & [0]_{u_1u_3} \\ [0]_{u_3\theta} & [0]_{u_3w} & [0]_{u_3u_1} & [0]_{u_3u_3} \end{bmatrix} \quad (31)$$

That

$$\mathbf{A}_{\theta\theta} = \begin{bmatrix} l_{\theta\theta 0} A_{L0} & [0] \\ [0] & l_{\theta\theta 1} A_{L1} \end{bmatrix}$$

$$\mathbf{A}_{\theta w} = \begin{bmatrix} l_{\theta h 0} A_{L0} & [0] \\ [0] & l_{\theta h 1} A_{L1} \end{bmatrix}$$

$$\mathbf{A}_{w\theta} = \begin{bmatrix} l_{h\theta 0} A_{L0} & [0] \\ [0] & l_{h\theta 1} A_{L1} \end{bmatrix}$$

$$\mathbf{A}_{ww} = \begin{bmatrix} l_{hh 0} A_{L0} & [0] \\ [0] & l_{hh 1} A_{L1} \end{bmatrix} \quad (32)$$

Also  $\mathbf{g} = \omega^2$  and  $\bar{\mathbf{q}}$  are eigenvalues and eigenvectors, sequentially. When there is no aerodynamic effect, the properties of free vibrations such as normal frequency and damping factor can be calculated, The relation between  $\mathbf{g}$  and  $\omega$  is specified by:

$$i\omega = i\sqrt{\mathbf{g}} = \mathbf{r} \pm i\bar{\omega} \quad (33)$$

The imaginary part indicates the natural frequency and the real part indicates the damping of the system.

The flutter instability of the cascade can be determined by plotting the damping of the system for a range of reduced frequencies. The flutter occurs when the sign of the damping changes from negative to positive. Its means when the real part becomes zero, the

phenomenon of flutter occurs. Non-Dimensional flutter speed is written as follows

$$\bar{U}_F = \frac{U_F}{b\omega_0} = \frac{\bar{\omega}_F/\omega_0}{k_F} \quad (34)$$

$\omega_0$  is the reference frequency,  $U_F$  is the flutter speed.  $k_F$  and  $\bar{\omega}_F$  are reduced frequency and natural frequency, respectively when flutter occurs.

### 3- Validation

To evaluate the accuracy of this study, the results from this study are verified by comparing the results with those available in the literature for several cases.

By comparing the values of torsional stiffness with the values of stress at the free edges and the middle plate (points corresponding to  $z = \frac{h}{2}, y = 0$  and  $z = 0, y = b$ ) in Swanson study [30], where a 4-layer beam with surface It is considered a rectangular section and has geometric and mechanical Properties according to Table 1, an acceptable match is observed between the results (Table 2).

In order, to evaluate the results of vibration analysis, the results of the natural frequency of the three-layer beam, which are obtained analytically and considering the twisting hypothesis of Saint-Venant's Principle and have similar properties and are made of aluminum, are compared [31] (Table 3).

In order to validate the aeroelasticity, the results of the graph related to the fuzzy diagram of a row of blades [16] and the aerodynamic coefficients in Whitehead study [29] have been compared. As can be seen at Table 4 and Figure 5, there is a good agreement between the results.

**Table 1 Geometric and mechanical Properties of the beam ([30])**

Parameter	unit	value
$G_{xz}$	GPa	131
$E_{zz}$	GPa	11.2
$E_{yy}$	GPa	131
$G_{xy}$	GPa	33.16
Total thickness	mm	5.2832
width	mm	50

**Table 2 Comparison of torsional constant and shear stresses**

Lay up	(Torsional constant) $GJ$			(Shear stress) $\tau_{xy}$			(Shear stress) $\tau_{xz}$		
	Swanson [30]	Present Study	Differences (%)	Swanson [30]	Present Study	Differences (%)	Swanson [30]	Present Study	Differences (%)
A[ $\pm 45/0/0/\pm 45$ ]	62.5	62.36	0.22	27.9	28.49	2.07	7.99	8.07	1
B[ $0/\pm 45/\pm 45/0$ ]	22.3	22.14	0.72	15.3	16.17	5.69	16.75	17.05	1.79

**Table 3 Comparison of the natural frequency of three-layer beams**

Mode number	Natural frequencies (Hz)		Difference %
	Present	Rao [31]	
1	250.69	250.61	0.03
2	754.13	751.84	0.30
3	1263.68	1253.06	0.85
4	1853.348	1819.85	1.84

**Table 4 Comparison of aerodynamic coefficients**

$\beta/2\pi$		$C_{Fq}$		$C_{F\alpha}$		$C_{Mq}$		$C_{M\alpha}$	
		Re	Im	Re	Im	Re	Im	Re	Im
0	Whitehead [29]	-0.3045	-0.0365	-0.3009	-0.0864	-0.0550	-0.0185	-0.0529	-0.0394
	Present study	-0.30451	-0.03648	-0.30093	-0.08637	-0.05503	-0.01838	-0.05291	-0.033
0.3	Whitehead [29]	-1.1140	0.1210	-1.1343	-0.0423	-0.2977	0.0196	-0.3016	0.0367
	Present study	-1.11394	0.121105	-1.13433	-0.04212	-0.29763	0.020122	-0.30156	-0.0362
0.6	Whitehead [29]	-1.2303	0.1178	-1.2500	-0.0605	-0.3390	0.0195	-0.3428	-0.0425
	Present study	-1.2302	0.117962	-1.25008	-0.06029	-0.33886	0.020086	-0.34277	-0.04194

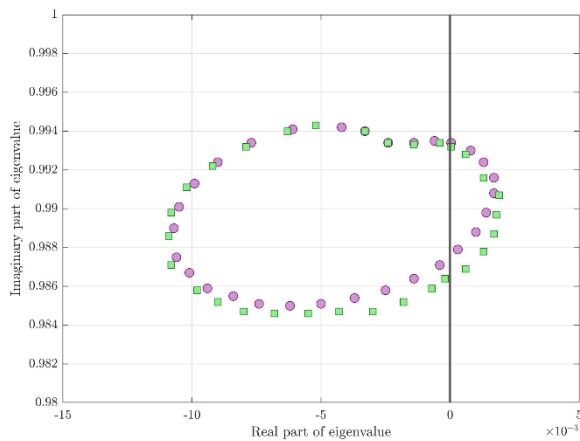


Fig.5 Fuzzy diagram of a row of blades [16]

Table 5 Parameters of a row of blades in the present study			
Parameter	unit	value	
length	mm	400	
width	mm	80	
Middle layer thickness	mm	1	
Elastic layer thickness	mm	1	
Young's modulus	GPa	72	
Elastic layers density	kg/m <sup>3</sup>	2700	
Middle layer density	kg/m <sup>3</sup>	3500	
Poisson ratio	-	0.3	
Disc radius	mm	300	
Fluid density	kg/m <sup>3</sup>	1	
Number of blades	-	56	
Stagger angle	degree	54.4	
Rotating speed	rpm	3000	
(m <sub>e</sub> ) Smart layer constant	pa.mm/kV	1500	
(m <sub>c</sub> ) Smart layer constant	mpa.s.mm/kV	270	
(b <sub>e</sub> ) Smart layer constant	-	0	
(b <sub>c</sub> ) Smart layer constant	pa.s	3.73	
Moment of inertia	m <sup>4</sup>	1/12(bh <sup>3</sup> )	
Elastic axis(a)	-	0	
Number of modes	-	5	

#### 4- Results and discussion

In this section the aero-elastic behavior of the blade with middle smart layer will be investigate. This review includes the investigation of the variation of real part and imaginary part of response with reduced frequency. Also in the following the flutter speed changes with electric field intensity will be reviewed. The effective parameters used in this section, are shown in Table 5.

It should be noted that the branch corresponding to each interblade phase angle mode becomes unstable at a specific reduced frequency. The critical phase angle mode is defined as the mode that becomes unstable earlier than the others. The reduced frequency at the instability point is referred to as the critical reduced frequency, or

flutter reduced frequency, and the corresponding speed is termed the critical speed or flutter speed. Since, in the present study, the number of interblade phase angle modes equals the number of blades (56 blade), plotting all of them in a single diagram would lead to visual clutter and obscure the presentation of results. Therefore, in what follows, only the results corresponding to the interblade phase angle mode that first undergoes flutter (i.e., the critical phase angle mode) are considered

##### 4-1- Torsional aeroelasticity

In this section, the torsional aero-elasticity of the blade row with the intelligent middle layer is analyzed. First, the diagrams of the real and imaginary parts of frequency without the smart layer are seen in Figure 6. It was noted that the flutter phenomenon occurs when the real part of eigenvalue becomes zero. It can be seen that in this case the point of occurrence of the flutter at the reduced frequency is 1.5.

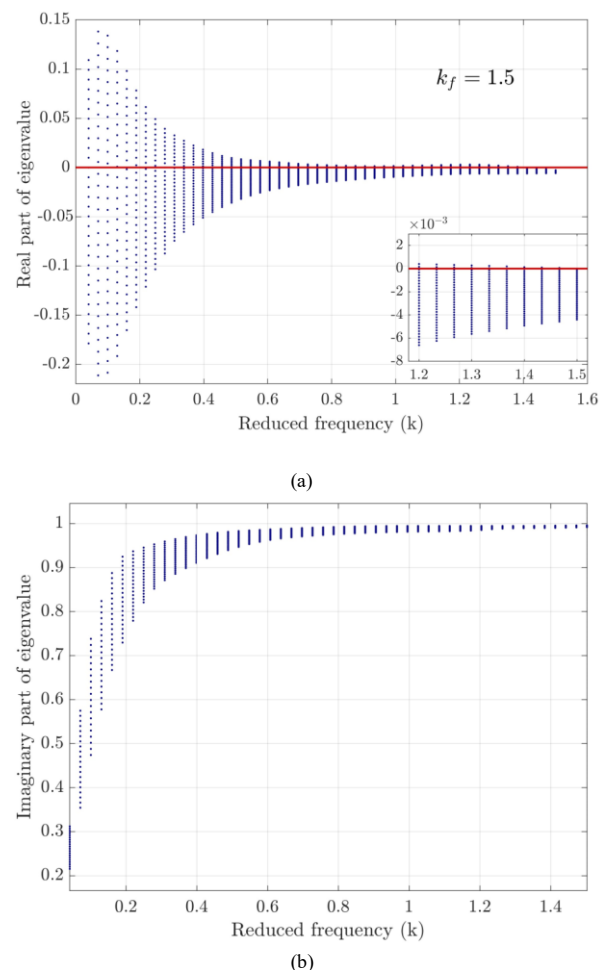
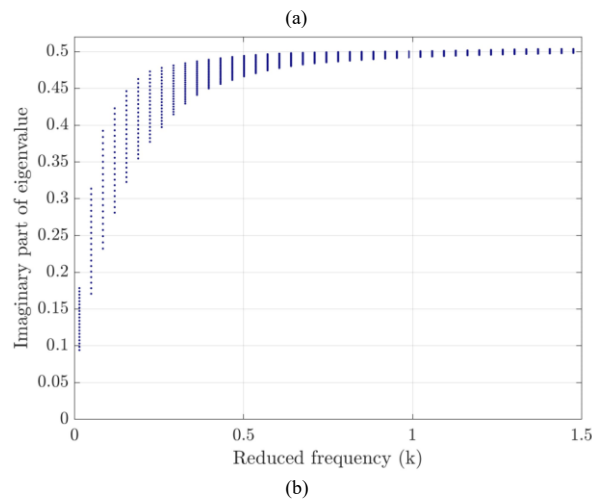
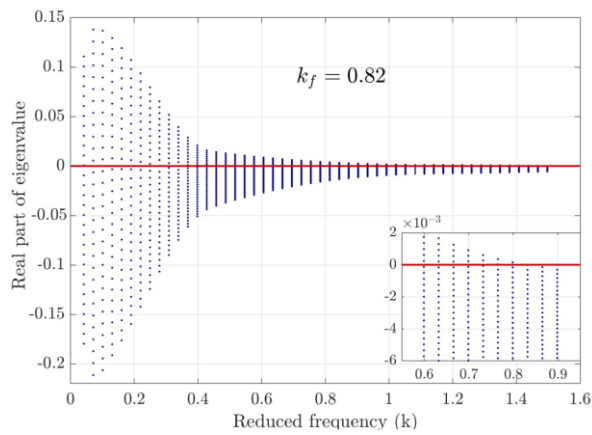


Fig.6 Variation of real part of eigenvalue (a) and imaginary part of eigenvalue with reduced frequency (k) for a row of blades without the middle smart layer

In the following, the addition of the middle layer in torsional aeroelasticity is investigated. Figure 7 shows the real and imaginary frequency diagrams in terms of reduced frequency in  $E= 5 \text{ Kv/mm}$ .





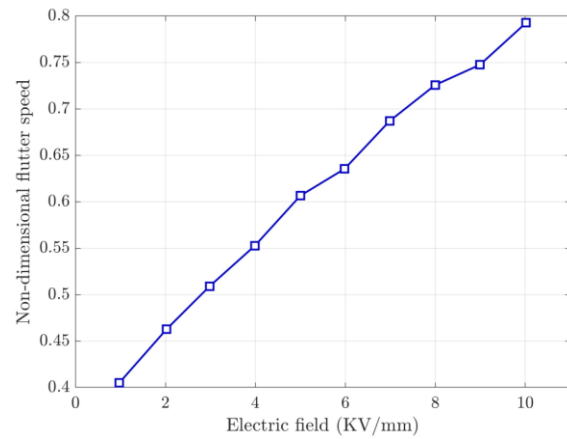
**Fig.7** Variation of real part of eigenvalue (a) and imaginary part of eigenvalue with reduced frequency ( $k$ ) for a row of blades with the middle smart layer by applying  $E=5$  kV/mm

As mentioned, the addition of a smart layer of electrorheology delays the flutter phenomenon and it is observed that the flutter point reaches from 1.5 to 0.82, and this reduction increases the flutter speed.

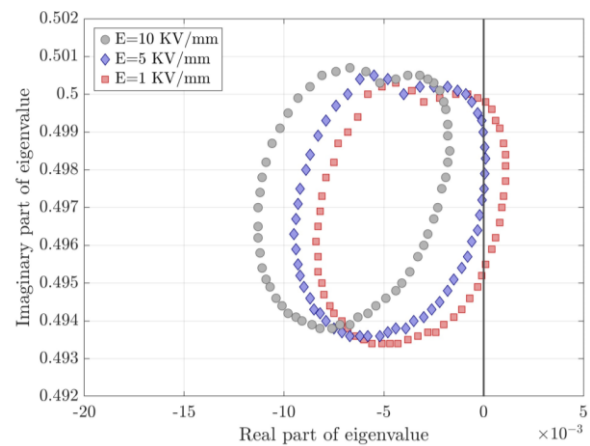
The increase in non-dimensional flutter speed based on the increase in electric field is shown in Figure 8. Increasing the electric field makes the middle smart layer harder and consequently the loss modulus increases and the flutter speed also increases.

Figure 9, shows the graph of the imaginary part in terms of the real part of the eigenvalue at a reduced frequency of 0.8. This figure shows that at this reduced frequency and in the electric field 1Kv/mm and 5 kV/mm, a number of blades are in an unstable state, but with the increase of the electric field to 10kV/mm, all the blades are in a stable state.

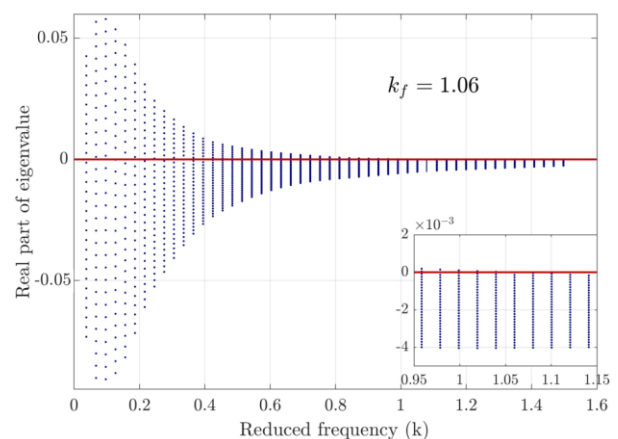
One of the effective parameters that has its effect on the aero-elastic behavior of the blades is the change in the length of the blades. By changing the blade length from 400mm to 800mm, the real and imaginary parts of the eigenvalue are shown in Figure 10. It is observed that this increase in length changes the point of the flutter and subsequently reduces the speed of the flutter.



**Fig.8** Non-dimensional speed of the flutter according to the increase of the electric field.



**Fig.9** Fuzzy diagram of the eigenvalue at a reduced frequency of 0.8





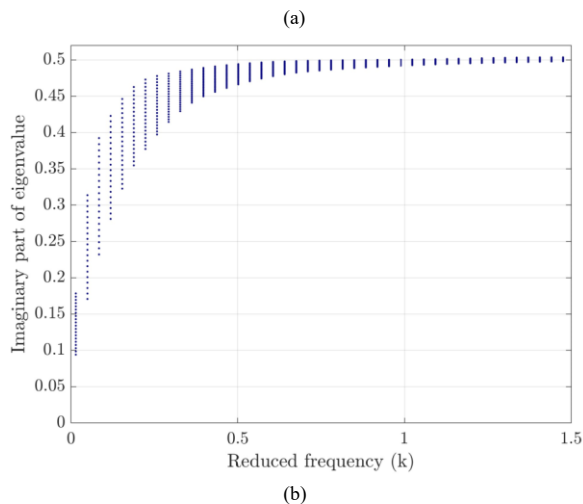


**Fig.10** Variation of real part of eigenvalue (a) and imaginary part of eigenvalue with reduced frequency ( $k$ ) for a row of blades with the middle smart layer by applying  $E=5$  kV/mm and blade length =8 mm.

#### 4-2- Bending- torsion coupling aeroelasticity

In this section, the effect of bending-torsion coupling on aeroelasticity is investigated. In Figure 11, the point of occurrence of the flutter phenomenon changes with increasing electric field 5kV/mm similar to the state of torsional aero-elasticity, and this indicates the delay of this phenomenon. It is observed that in this case, instability occurs in the torsion mode, and in the imaginary part, which represents the frequency, it is more in this mode than the bending mode. Compared to the uncoupled state of torsion, it is observed that the reduced frequency at which the flutter occurs has increased slightly, which is due to the fact that in the case of bending the aerodynamic forces on the structure increase and then the flutter will occur sooner. Also, the dimensionless speed of the flutter is depicted in the bending-twisting coupling mode in Figure 12. Due to the fact that in the present study and the parameters used, it was observed that the flutter occurred in the torsional mode, the speed of the flutter in bending-torsion coupling mode is slightly different from the torsional aeroelasticity mode.

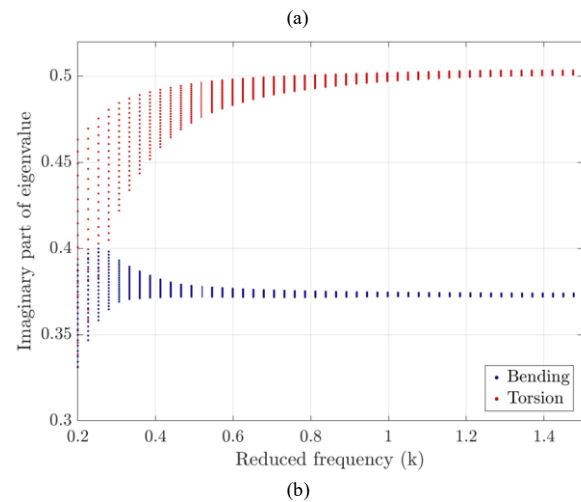


**Fig.11** Variation of real part of eigenvalue (a) and imaginary part of eigenvalue with reduced frequency ( $k$ ) for a row of blades with the middle smart layer in bending-torsion coupling aeroelasticity by applying  $E=5$  kV/mm.

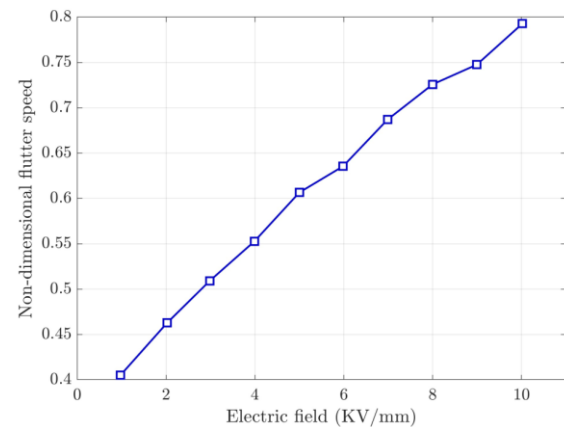
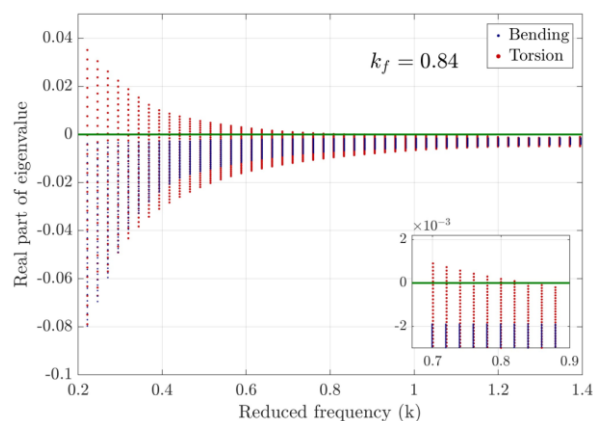


**Fig.12** Variation of non-dimensional flutter speed by increase the electric field in bending-torsion coupling aeroelasticity.



#### 4- Conclusion

In this work, the aero-elasticity and flutter instability of a single row blade with electrorheological smart fluid have been studied. The blades are considered as a three-layer beam with two elastic layers and a smart middle layer. Aerodynamic modeling is performed using Whitehead's unsteady theory. In this theory, the flow around the blades is subsonic and incompressible. Due to the fact that the cross section of the blade is geometrically symmetrical, the bending and torsional vibrations are uncoupled but coupled due to the aerodynamic effect. Using the assumed mode method with Lagrange equations, the governing equation of motion of the coupled system is derived. The instability of the system is investigated by changing the intensity of the electric field. Electrorheological smart fluid as middle layer improves aeroelastic behavior. This fluid has a behavior similar to viscoelastic fluids and the loss modulus delays the flutter phenomenon and increases the flutter speed. As the electric field intensifies from 4 to 6, the dimensionless speed of the flutter increases by 20%. It was also observed that increasing the blade length reduces the flutter speed. And the reduced frequency point of the flutter increases in the real part diagram of the eigenvalue.

## Nomenclature

$A_k$	area of cross-section, ( $k = 1, 2, 3$ )	$U_F$	flow velocity at flutter point
$a$	elastic axis location, ( $a = 0$ )	$\bar{U}_F$	nondimensional flow velocity at flutter point
$b$	blade half-width	$U_{1,2,3}$	potential energy terms
$b_0$	blade half-width at $x = 0$	$u_k$	axial displacements of the elastic layers, ( $k = 1, 3$ )
$c$	blade chord, ( $c = 2b$ )	$W_c$	work done by centrifugal force
$E$	Electric field intensity	$W_a$	work done by aerodynamic loadings
$E_k$	Young's modulus of different layers, ( $k = 1, 2, 3$ )	$w$	bending displacement
$G^*$	complex shear modulus	$XYZ$	disk-blade coordinate system
$G'$	storage modulus	$xyz$	blade coordinate system
$G''$	loss modulus	$xy'z'$	blade coordinate system ( $y'$ along rotating axis, $z'$ along circumferential direction)
$h$	total thickness of the blade	$\rho_k$	density of the layers, ( $k = 1, 2, 3$ )
$h_k$	thickness of the layers, ( $k = 1, 2, 3$ )	$\rho$	density of flow
$h_{ar}$	bending amplitude in the $r$ th mode	$\Omega$	rotating speed
$I$	identity matrix	$\omega$	frequency
$I_k$	second moment of area, ( $k = 1, 2, 3$ )	$\bar{\omega}$	imaginary part of the eigenvalue
$k$	reduced frequency	$\bar{\omega}_F$	imaginary part of the eigenvalue at flutter point
$k_F$	reduced frequency at flutter point	$\omega_0$	reference frequency
$L$	blade length	$\mu$	real part of the eigenvalue
$\bar{L}$	aerodynamic lift	$\theta$	torsional motion
$\bar{M}$	aerodynamic moment	$\theta_{ar}$	torsional amplitude in the $r$ th mode
$m$	mass per unit length	$\xi$	stagger angle
$N$	number of blades	$\eta_c$	loss factor of MRE material
$P(x)$	centrifugal force per unit area	$\phi_{mi}$	trial functions
$p(x)$	centrifugal force	$\gamma$	shear strain in MRE layer
$q_s$	vibration amplitude for the $s$ th blade	$\lambda$	reduced frequency parameter, ( $\lambda = 2k$ )
$q_{ar}$	vibration amplitude for the $r$ th mode	$\bar{\lambda}$	eigenvalue, Eq. (27)
$R$	disk radius	$\sigma_r$	inter-blade phase angle
$r$	integer specifying the mode of tuned cascade	$\sigma_{xz}$	shear stress, $xz$ component
$s$	integer specifying blade number	$\sigma_{xy}$	shear stress, $xy$ component
$T_{1,2,3,4}$	kinetic energy terms	$\psi_k$	warping function, ( $k = 1, 2, 3$ )
$t$	time	$l_{hr}, l_{h\theta r}$	lift coefficients due to bending and torsional motions
$U$	flow velocity	$l_{\theta hr}, l_{\theta\theta r}$	moment coefficients due to bending and torsional motions
		$C_{Fq}, C_{F\theta}, C_{Mq}, C_{M\theta}$	parameters defined in lift and moment coefficients

In addition, the results show that in the blade row, the flutter phenomenon occurs in the torsion mode, and considering the bending-torsion coupling, the point of occurrence of the flutter changes slightly, and this is because considering the bending-torsion coupling, Aerodynamic forces increase.

As an important conclusion it can be said that adding the electrorheological smart fluid to the sandwich beam structure can be considered as a passive method in controlling vibrations and delaying the flutter phenomenon.

**Ethics Approval:** The scientific content of this article is the result of the authors' research and has not been published in any Iranian or international journal.

**Conflict of Interest:** The authors declare that they have no conflict of interest.

## Appendix

For simplicity, it is assumed that the number of blades and the number of assumed modes are both equal to two. Initially, the generalized coordinates are defined as follows:

$$q = \begin{bmatrix} q_{\theta 1}^0 \\ q_{\theta 2}^0 \\ q_{\theta 1}^1 \\ q_{\theta 2}^1 \\ q_{w 1}^0 \\ q_{w 2}^0 \\ q_{w 1}^1 \\ q_{w 2}^1 \\ q_{u 1 1}^0 \\ q_{u 1 2}^0 \\ q_{u 1 1}^1 \\ q_{u 1 2}^1 \\ q_{u 3 1}^0 \\ q_{u 3 2}^0 \\ q_{u 3 1}^1 \\ q_{u 3 2}^1 \end{bmatrix} \quad (35)$$

It should be noted that the superscript denotes the blade number, while the subscript indicates the mode number. The torsional and longitudinal-bending mass and stiffness matrices for an arbitrary blade are expressed as follows:

$$M_{\theta}^r = \begin{bmatrix} M_{\theta 11}^r & M_{\theta 12}^r \\ M_{\theta 21}^r & M_{\theta 22}^r \end{bmatrix} \quad (36)$$

$$K_{\theta}^r = \begin{bmatrix} K_{\theta 11}^r & K_{\theta 12}^r \\ K_{\theta 21}^r & K_{\theta 22}^r \end{bmatrix} \quad (37)$$

$$M_b^r = \begin{bmatrix} M_{ww11}^r & M_{ww12}^r & M_{wu11}^r & M_{wu12}^r & M_{wu31}^r & M_{wu32}^r \\ M_{ww21}^r & M_{ww22}^r & M_{wu21}^r & M_{wu22}^r & M_{wu32}^r & M_{wu32}^r \\ M_{u1w11}^r & M_{u1w12}^r & M_{u1u11}^r & M_{u1u12}^r & M_{u1u31}^r & M_{u1u32}^r \\ M_{u1w21}^r & M_{u1w22}^r & M_{u1u21}^r & M_{u1u22}^r & M_{u1u32}^r & M_{u1u32}^r \\ M_{u3w11}^r & M_{u3w12}^r & M_{u3u11}^r & M_{u3u12}^r & M_{u3u31}^r & M_{u3u32}^r \\ M_{u3w21}^r & M_{u3w22}^r & M_{u3u21}^r & M_{u3u22}^r & M_{u3u32}^r & M_{u3u32}^r \end{bmatrix} \quad (38)$$

$$K_b^r = \begin{bmatrix} K_{ww11}^r & K_{ww12}^r & K_{wu11}^r & K_{wu12}^r & K_{wu31}^r & K_{wu32}^r \\ K_{ww21}^r & K_{ww22}^r & K_{wu21}^r & K_{wu22}^r & K_{wu32}^r & K_{wu32}^r \\ K_{u1w11}^r & K_{u1w12}^r & K_{u1u11}^r & K_{u1u12}^r & K_{u1u31}^r & K_{u1u32}^r \\ K_{u1w21}^r & K_{u1w22}^r & K_{u1u21}^r & K_{u1u22}^r & K_{u1u32}^r & K_{u1u32}^r \\ K_{u3w11}^r & K_{u3w12}^r & K_{u3u11}^r & K_{u3u12}^r & K_{u3u31}^r & K_{u3u32}^r \\ K_{u3w21}^r & K_{u3w22}^r & K_{u3u21}^r & K_{u3u22}^r & K_{u3u32}^r & K_{u3u32}^r \end{bmatrix} \quad (39)$$

By considering two blades, the overall mass matrix (**M**) and stiffness matrix (**K**) are obtained as follows:

$$M = \begin{bmatrix} M_{\theta 11}^0 & M_{\theta 12}^0 & 0 & 0 & 0 & 0 & 0 & 0 & 0 & 0 & 0 & 0 & 0 & 0 & 0 & 0 \\ M_{\theta 21}^0 & M_{\theta 22}^0 & 0 & 0 & 0 & 0 & 0 & 0 & 0 & 0 & 0 & 0 & 0 & 0 & 0 & 0 \\ 0 & 0 & M_{\theta 11}^1 & M_{\theta 12}^1 & 0 & 0 & 0 & 0 & 0 & 0 & 0 & 0 & 0 & 0 & 0 & 0 \\ 0 & 0 & M_{\theta 21}^1 & M_{\theta 22}^1 & 0 & 0 & 0 & 0 & 0 & 0 & 0 & 0 & 0 & 0 & 0 & 0 \\ 0 & 0 & 0 & 0 & M_{ww11}^0 & M_{ww12}^0 & 0 & 0 & M_{wu11}^0 & M_{wu12}^0 & 0 & 0 & M_{wu31}^0 & M_{wu32}^0 & 0 & 0 \\ 0 & 0 & 0 & 0 & M_{ww21}^0 & M_{ww22}^0 & 0 & 0 & M_{wu21}^0 & M_{wu22}^0 & 0 & 0 & M_{wu32}^0 & M_{wu32}^0 & 0 & 0 \\ 0 & 0 & 0 & 0 & 0 & 0 & M_{u1w11}^1 & M_{u1w12}^1 & 0 & 0 & M_{u1u11}^1 & M_{u1u12}^1 & 0 & 0 & M_{u1u31}^1 & M_{u1u32}^1 \\ 0 & 0 & 0 & 0 & 0 & 0 & M_{u1w21}^1 & M_{u1w22}^1 & 0 & 0 & M_{u1u21}^1 & M_{u1u22}^1 & 0 & 0 & M_{u1u32}^1 & M_{u1u32}^1 \\ 0 & 0 & 0 & 0 & M_{u3w11}^0 & M_{u3w12}^0 & 0 & 0 & M_{u3u11}^0 & M_{u3u12}^0 & 0 & 0 & M_{u3u31}^0 & M_{u3u32}^0 & 0 & 0 \\ 0 & 0 & 0 & 0 & M_{u3w21}^0 & M_{u3w22}^0 & 0 & 0 & M_{u3u21}^0 & M_{u3u22}^0 & 0 & 0 & M_{u3u32}^0 & M_{u3u32}^0 & 0 & 0 \\ 0 & 0 & 0 & 0 & 0 & 0 & M_{u1w11}^1 & M_{u1w12}^1 & 0 & 0 & M_{u1u11}^1 & M_{u1u12}^1 & 0 & 0 & M_{u1u31}^1 & M_{u1u32}^1 \\ 0 & 0 & 0 & 0 & 0 & 0 & M_{u1w21}^1 & M_{u1w22}^1 & 0 & 0 & M_{u1u21}^1 & M_{u1u22}^1 & 0 & 0 & M_{u1u32}^1 & M_{u1u32}^1 \\ 0 & 0 & 0 & 0 & M_{u3w11}^0 & M_{u3w12}^0 & 0 & 0 & M_{u3u11}^0 & M_{u3u12}^0 & 0 & 0 & M_{u3u31}^0 & M_{u3u32}^0 & 0 & 0 \\ 0 & 0 & 0 & 0 & M_{u3w21}^0 & M_{u3w22}^0 & 0 & 0 & M_{u3u21}^0 & M_{u3u22}^0 & 0 & 0 & M_{u3u32}^0 & M_{u3u32}^0 & 0 & 0 \\ 0 & 0 & 0 & 0 & 0 & 0 & M_{u3w11}^1 & M_{u3w12}^1 & 0 & 0 & M_{u3u11}^1 & M_{u3u12}^1 & 0 & 0 & M_{u3u31}^1 & M_{u3u32}^1 \\ 0 & 0 & 0 & 0 & 0 & 0 & M_{u3w21}^1 & M_{u3w22}^1 & 0 & 0 & M_{u3u21}^1 & M_{u3u22}^1 & 0 & 0 & M_{u3u32}^1 & M_{u3u32}^1 \end{bmatrix} \quad (40)$$

$$K = \begin{bmatrix} K_{\theta 11}^0 & K_{\theta 12}^0 & 0 & 0 & 0 & 0 & 0 & 0 & 0 & 0 & 0 & 0 & 0 & 0 & 0 & 0 \\ K_{\theta 21}^0 & K_{\theta 22}^0 & 0 & 0 & 0 & 0 & 0 & 0 & 0 & 0 & 0 & 0 & 0 & 0 & 0 & 0 \\ 0 & 0 & K_{\theta 11}^1 & K_{\theta 12}^1 & 0 & 0 & 0 & 0 & 0 & 0 & 0 & 0 & 0 & 0 & 0 & 0 \\ 0 & 0 & K_{\theta 21}^1 & K_{\theta 22}^1 & 0 & 0 & 0 & 0 & 0 & 0 & 0 & 0 & 0 & 0 & 0 & 0 \\ 0 & 0 & 0 & 0 & K_{ww11}^0 & K_{ww12}^0 & 0 & 0 & K_{wu11}^0 & K_{wu12}^0 & 0 & 0 & K_{wu31}^0 & K_{wu32}^0 & 0 & 0 \\ 0 & 0 & 0 & 0 & K_{ww21}^0 & K_{ww22}^0 & 0 & 0 & K_{wu21}^0 & K_{wu22}^0 & 0 & 0 & K_{wu32}^0 & K_{wu32}^0 & 0 & 0 \\ 0 & 0 & 0 & 0 & 0 & 0 & K_{u1w11}^1 & K_{u1w12}^1 & 0 & 0 & K_{u1u11}^1 & K_{u1u12}^1 & 0 & 0 & K_{u1u31}^1 & K_{u1u32}^1 \\ 0 & 0 & 0 & 0 & 0 & 0 & K_{u1w21}^1 & K_{u1w22}^1 & 0 & 0 & K_{u1u21}^1 & K_{u1u22}^1 & 0 & 0 & K_{u1u32}^1 & K_{u1u32}^1 \\ 0 & 0 & 0 & 0 & K_{u3w11}^0 & K_{u3w12}^0 & 0 & 0 & K_{u3u11}^0 & K_{u3u12}^0 & 0 & 0 & K_{u3u31}^0 & K_{u3u32}^0 & 0 & 0 \\ 0 & 0 & 0 & 0 & K_{u3w21}^0 & K_{u3w22}^0 & 0 & 0 & K_{u3u21}^0 & K_{u3u22}^0 & 0 & 0 & K_{u3u32}^0 & K_{u3u32}^0 & 0 & 0 \\ 0 & 0 & 0 & 0 & 0 & 0 & K_{u1w11}^1 & K_{u1w12}^1 & 0 & 0 & K_{u1u11}^1 & K_{u1u12}^1 & 0 & 0 & K_{u1u31}^1 & K_{u1u32}^1 \\ 0 & 0 & 0 & 0 & 0 & 0 & K_{u1w21}^1 & K_{u1w22}^1 & 0 & 0 & K_{u1u21}^1 & K_{u1u22}^1 & 0 & 0 & K_{u1u32}^1 & K_{u1u32}^1 \\ 0 & 0 & 0 & 0 & K_{u3w11}^0 & K_{u3w12}^0 & 0 & 0 & K_{u3u11}^0 & K_{u3u12}^0 & 0 & 0 & K_{u3u31}^0 & K_{u3u32}^0 & 0 & 0 \\ 0 & 0 & 0 & 0 & K_{u3w21}^0 & K_{u3w22}^0 & 0 & 0 & K_{u3u21}^0 & K_{u3u22}^0 & 0 & 0 & K_{u3u32}^0 & K_{u3u32}^0 & 0 & 0 \\ 0 & 0 & 0 & 0 & 0 & 0 & K_{u3w11}^1 & K_{u3w12}^1 & 0 & 0 & K_{u3u11}^1 & K_{u3u12}^1 & 0 & 0 & K_{u3u31}^1 & K_{u3u32}^1 \\ 0 & 0 & 0 & 0 & 0 & 0 & K_{u3w21}^1 & K_{u3w22}^1 & 0 & 0 & K_{u3u21}^1 & K_{u3u22}^1 & 0 & 0 & K_{u3u32}^1 & K_{u3u32}^1 \end{bmatrix} \quad (41)$$

The aerodynamic coupling matrix is also defined as follows:

$$\bar{A} = \begin{bmatrix} \pi \rho b^4 E A_{\theta\theta} E^{-1} & \pi \rho b^3 E A_{\theta w} E^{-1} & [0]_{\theta u_1} & [0]_{\theta u_3} \\ \pi \rho b^3 E A_{w\theta} E^{-1} & \pi \rho b^2 E A_{ww} E^{-1} & [0]_{wu_1} & [0]_{wu_3} \\ [0]_{u_1\theta} & [0]_{u_1w} & [0]_{u_1u_1} & [0]_{u_1u_3} \\ [0]_{u_3\theta} & [0]_{u_3w} & [0]_{u_3u_1} & [0]_{u_3u_3} \end{bmatrix} \quad (42)$$

This matrix has the same dimensions as matrices **M** and **K**, where [0] denotes the zero matrix with dimensions corresponding to the degrees of freedom, and **E** represents the mistuning matrix in a single row of blades.

## References

- [1] Ceardle, J. "Whirl flutter of turboprop aircraft structures", Woodhead Publishing. (2015).
- [2] Dugeai, A., Mauffrey, Y., Placzek, A., Verley, S. "Overview of the Aeroelastic Capabilities of the elsA Solver within the Context of Aeronautical Engines", Journal Aerospace Lab, 14 (2018). Doi. 10.12762/2018.AL14-03
- [3] Casoni, M., Magrini, A., & Benini, E. "Multi-Frequency Aeroelastic ROM for Transonic Compressors", *Aerospace*, 11(12), pp. 1036 (2024). <https://doi.org/10.3390/aerospace11121036>
- [4] Munteanu, L., Munteanu, A., Sedlacik, M., "Electrorheological fluids: A living review", *Progress in Materials Science*, 151 (2025). doi.org/10.1016/j.pmatsci.2024.101421.

- [5] Edward, M., Kerwin, Jr. "Damping of flexural waves by a constrained viscoelastic layer", *The Journal of the Acoustical Society of America*, **31**, pp. 952-962 (1959). Doi.org/10.1121/1.1907821
- [6] Qiu, J., Tani, J., Hajika, T. "Damping effect of multi-layer beams with embedded electro-rheological fluid", *Journal of intelligent material systems & structures*, **10**, pp. 521-529 (1999). Doi.org/10.1106/R4HQ-F2M0-QGY3-NVV8
- [7] Kang, Y.K., Kim, J., Choi, S.B. "Passive and active damping characteristics of smart electro-rheological composite beams", *Smart materials and structures*, **10**, 724 (2001). Doi.org/10.1088/0964-1726/10/4/316
- [8] Wei, K., Meng, G., Lu, H., Zhu, S. "Dynamic analysis of rotating electrorheological composite beams", *International Journal of Modern Physics B*, **19**, pp. 1236-1242 (2005). Doi.org/10.1142/S0217979205030128
- [9] Arikoglu, A., Ozkol, I. "Vibration analysis of composite sandwich beams with viscoelastic core by using differential transform method", *Composite Structures*, **92**, pp. 3031-3039 (2010). Doi.org/10.1016/j.compstruct.2010.05.022
- [10] Allahverdizadeh, A., Mahjoob, M., Eshraghi, I., Nasrollahzadeh, N. "On the vibration behavior of functionally graded electrorheological sandwich beams", *International Journal of Mechanical Sciences*, **70**, pp. 130-139 (2013). Doi.org/10.1016/j.ijmecsci.2013.02.011
- [11] Marshall, J., Imregun, M. "A review of aeroelasticity methods with emphasis on turbomachinery applications", *Journal of fluids and structures*, **10**(3), pp. 237-267 (1996). Doi.org/10.1006/jfls.1996.0015
- [12] Whitehead, D.S. "Bending flutter of unstalled cascade blades at finite deflection", (1962). <https://reports.aerade.cranfield.ac.uk/handle/1826.2/3968>
- [13] Rahiminasab, J., Rezaeepazhand, J. "Aeroelastic stability of smart sandwich plates with electrorheological fluid core and orthotropic faces", *Journal of Intelligent Material Systems and Structures*, **24**(5), 669-677 (2013). Doi.org/10.1177/1045389X12470306
- [14] Brahimi, F., Ouibrahim, A. "Blade dynamical response based on aeroelastic analysis of fluid structure interaction in turbomachinery", *Energy*, **115**, pp. 986-995 (2016). Doi.org/10.1016/j.energy.2016.09.071
- [15] Bornassi, S., Navazi, H., Haddadpour, H. "Coupled bending-torsion flutter investigation of MRE tapered sandwich blades in a turbomachinery cascade", *Thin-Walled Structures*, **152**, pp. 106765 (2020). Doi.org/10.1016/j.tws.2020.106765
- [16] Kaza, K., Kielb, R.E. "Effects of mistuning on bending-torsion flutter and response of a cascade in incompressible flow", *NTRS-NASA Technical Reports Server*, (1981). <https://ntrs.nasa.gov/citations/19810007977>
- [17] Kielb, R.E., Kaza, K. "Aeroelastic characteristics of a cascade of mistuned blades in subsonic and supersonic flows", *NTRS-NASA Technical Reports Server*, (1983). <https://ntrs.nasa.gov/citations/19810017955>
- [18] Mutra, R.R., Srinivas, J. "Active Vibration Control in Turbocharger Rotor System with the Use of Electromagnetic Actuator", *Advances in Applied Mechanical Engineering*. Lecture Notes in Mechanical Engineering. Springer, Singapore, pp. 563-570 (2020). [https://doi.org/10.1007/978-981-15-1201-8\\_63](https://doi.org/10.1007/978-981-15-1201-8_63)
- [19] Sakly, F., Chouchane, M. "Vibration control of a bi-disk rotor using electro-rheological elastomers", *Smart materials and structures*, **31**(6) (2022). DOI 10.1088/1361-665X/ac691a.
- [20] Liu, W., Jin, H., Yao, J. "Vibration performance analysis of a self-energized damper composed of electrorheological fluid and piezoelectric ceramics", *Mechanics Based Design of Structures and Machines*, **51**(10), pp. 5968-5982 (2022). <https://doi.org/10.1080/15397734.2022.2027781>
- [21] Choi, Y., Cho, J., Choi, S., Wereley, N. "Constitutive models of electrorheological and magnetorheological fluids using viscometers", *Smart materials and structures*, **14**(5), pp. 1025 (2005). Doi.org/10.1088/0964-1726/14/5/041
- [22] Weiss, K.D., Carlson, J.D., Nixon, D.A. "Viscoelastic properties of magneto-and electro-rheological fluids", *Journal of Intelligent Material Systems and Structures*, **5**(6), pp. 772-775 (1994). Doi.org/10.1177/1045389X94005006
- [23] Yalcintas, M., Dai, H. "Vibration suppression capabilities of magnetorheological materials based adaptive structures", *Smart Materials and Structures*, **13**(1) (2004). Doi.org/10.1088/0964-1726/13/1/001
- [24] Wei, K., Bai, Q., Meng, G., Ye, L. "Vibration characteristics of electrorheological elastomer sandwich beams", *Smart Materials and Structures*, **20**(5), pp. 055-012 (2011). Doi.org/10.1088/0964-1726/20/5/055012
- [25] Lane, F. "System mode shapes in the flutter of compressor blade rows", *Journal of the Aeronautical Sciences*, **23**(1), pp. 54-66 (1956). Doi.org/10.2514/8.3502
- [26] Savoia, M., Tullini, N. "Torsional response of inhomogeneous and multilayered composite beams", *Composite Structures*, **25**(1-4), pp. 587-594 (1993). Doi.org/10.1016/0263-8223(93)90207-7
- [27] Bornassi, S., Navazi, H.M. "Torsional vibration analysis of a rotating tapered sandwich beam with magnetorheological elastomer core", *Journal of Intelligent Material Systems and Structures*, **29**(11), 2406-2423 (2018). Doi.org/10.1177/1045389X18770864
- [28] Mead, D., Markus, S. "The forced vibration of a three-layer, damped sandwich beam with arbitrary boundary conditions", *Journal of sound and vibration*, **10**(2) pp. 163-175 (1969). Doi.org/10.1016/0022-460X(69)90193-X
- [29] Whitehead, D.S. "Force and moment coefficients for vibrating airfoils in cascade", *Aeronautical Research Council Reports & Memoranda* (1962). <https://reports.aerade.cranfield.ac.uk/handle/1826.2/3828>
- [30] Swanson, S.R. "Torsion of laminated rectangular rods. Composite structures", **42** pp. 23-31 (1998). Doi.org/10.1016/S0263-8223(98)00055-5
- [31] Rao, S.S. "Vibration of continuous systems", *Wiley Online Library* (2007). Doi.org/10.1002/9780470117866